

SDM Optical Systems with MMSE Equalizers: Information Rates and Performance Monitoring

Lucas Alves Zischler, *Graduate Student Member, IEEE*, and Darli A. A. Mello, *Member, IEEE*

Abstract—The information rate of coupled space-division multiplexing (SDM) transmission systems is impaired by the stochastic effects of mode-dependent gain (MDG) and mode-dependent loss (MDL), turning it into a random variable and reducing its average value. In systems operating with minimum mean squared error (MMSE) equalizers and no channel-state information (CSI), co-channel interference further reduces the instantaneous and average information rates. Analytical solutions for the average information rate in MDG- and MDL-impaired systems under strong coupling have been presented in early studies assuming ideal maximum-likelihood (ML) equalization. However, a solution encompassing co-channel interference under MMSE equalization has not been presented yet. In this work, we derive statistical models for the MMSE equalizer coefficients and develop analytical solutions for the post-filtering information rate. We also use these statistical models and analytical solutions to carry out MDG and signal-to-noise ratio (SNR) monitoring in coupled SDM systems. The derived analytical solutions and monitoring techniques are validated by Monte-Carlo simulations, exhibiting a suitable accuracy within practical operational values.

Index Terms—Space-division multiplexing, MIMO MMSE equalization, information rate, performance monitoring.

I. INTRODUCTION

NOVEL system designs for space-division multiplexing (SDM) transmission have been proposed as a possible step to support the sustained traffic growth in optical networks, particularly in the long-haul and submarine spaces [1]–[7]. In these systems, few-mode fibers (FMFs) and multi-core fibers (MCFs) use multiple spatial channels to increase throughput. However, in coupled propagation schemes, such as those employing FMFs or coupled-core MCFs, deviations in per-mode¹ gains and attenuations result in the effects of mode-dependent gain (MDG) and mode-dependent loss (MDL)². In the presence of random mode coupling, these effects become stochastic and reduce average information rates [8]–[10].

Coupled SDM systems require multiple-input multiple-output (MIMO) receivers to unravel the transmitted signals

that are mixed during transmission. These receivers typically implement minimum mean squared error (MMSE) equalizers owing to their suitable convergence properties, simple feed-forward implementation, and low complexity. However, MIMO equalizers operating under the MMSE criteria further penalize the information rate of MDG-impaired systems due to unmitigated co-channel interference [12]. While analytical solutions for the information rates of MDG-impaired systems under ideal maximum-likelihood (ML) equalization have been presented in [13, Eq. (10)] and [9, Eq. (12)], models accounting for the co-channel interference generated in MMSE equalization are still an open problem.

In this paper, we extend [11] and derive in detail an analytical expression for the information rate of coupled SDM systems under MMSE equalization. The derivations are based on the works by Ho and Kahn in [14] and [13], which show that, in SDM systems with strong coupling, the group delay and modal gains in logarithmic scale follow fixed-trace Gaussian unitary ensemble (GUE) random matrices. GUE random matrices have been extensively studied in other fields of physics and mathematics [15]–[18]. The derived expression is exact at the limiting case of an infinite number of supported modes. For a practical number of mode counts, the model provides a valid approximation for average information rate metrics. We apply the analytical method to estimate capacity, pre-forward error correction (FEC) bit-error rate (BER), and constrained capacity considering particular modulation formats. Following the approach in [13], [19]–[21], and for the sake of clarity, we neglect the effect of nonlinearities, setting an upper bound on capacity. Linear propagation is particularly relevant for current SDM submarine systems that are not limited by nonlinearities but by power-feed constraints. For further developments on the nonlinearity modeling in SDM systems, please see [22], [23].

This work is structured as follows. Section II briefly reviews MIMO MMSE equalizers, their relation to the optical channel, and the statistics of the channel power gains. Section III presents the analytical solution for the post-filtering signal-to-interference-plus-noise ratio (SINR) as a function of the pre-filtering signal-to-noise ratio (SNR) and MDG, and relates the post-filtering SINR to information rate metrics assuming an additive white Gaussian noise (AWGN) channel. Section IV associates the power gain statistics to the MIMO MMSE equalizer inverse eigenvalues, and uses the derived analytical formulas for performance monitoring and parameter estimation. Lastly, Section V concludes the paper.

Manuscript received XXX xx, XXXX; revised XXXXX xx, XXXX; accepted XXXX XX, XXXX. This work was financed in part by the Coordenação de Aperfeiçoamento de Pessoal de Nível Superior – Brasil (CAPES) – Finance Code 001, CNPq, and Fapesp grant #2022/11596-0. (Corresponding author: Lucas Alves Zischler).

Parts of this work appear in Zischler et al. [11].

L. Alves Zischler is with the Department of Physical and Chemical Sciences, University of L'Aquila, L'Aquila 67100, Italy; (e-mail: lucas.zischler@univaq.it).

D. A. A. Mello is with the School of Electrical and Computer Engineering, State University of Campinas, Campinas 13083-970, Brazil.

¹In this work, the term "mode" is used to refer to any supported orthogonal spatial or polarization channel, such as linearly polarized (LP) modes, polarizations, or cores.

²MDG and MDL effects are addressed by the same mathematical modeling. Therefore, in this work, we refer to both phenomena as simply MDG.

II. MIMO MMSE EQUALIZATION FUNDAMENTALS

A. Equalizer matrix

In coupled SDM links, the optical channel operating in the linear domain can be modeled as a frequency-dependent transfer matrix $\mathbf{H}(\omega) \in \mathbb{C}^{D \times D}$, where D is the number of supported polarization and spatial modes. In the derivations, as we calculate averages, we omit the frequency dependence of \mathbf{H} without lack of generality. The considered channel model assumes that the noise is additive and can be accounted independently of the modal coupling matrix \mathbf{H} . Under such consideration, we can replace all distributed additive noise sources with an equivalent additive source at the receiver side.

As the transmitted signals couple during propagation, a MIMO equalizer is required at the receiver to orthogonalize the incoming streams and recover the transmitted data. Practical MIMO equalizers typically employ the MMSE criteria owing to the low implementation complexity of least mean squares (LMS) filters.

The coefficients of the MIMO MMSE equalizer, for a particular spectral component, $\mathbf{W} \in \mathbb{C}^{D \times D}$, relate to the channel transfer matrix, $\mathbf{H} \in \mathbb{C}^{D \times D}$, by [24, Eq. (6.44)]

$$\mathbf{W} = \left(\mathbf{H}^H \mathbf{H} + \frac{\mathbf{I}}{\text{SNR}} \right)^{-1} \mathbf{H}^H, \quad (1)$$

where SNR is the ratio between total pre-filtering signal power and total AWGN power over all D modes. In a high SNR scenario, the equalizer matrix approaches the channel matrix inverse ($\lim_{\text{SNR} \rightarrow \infty} \mathbf{W} = \mathbf{H}^{-1}$).

In coupled SDM systems, the SNR accepts several different definitions. In general, in-line SDM amplifiers are usually designed to have a controlled gain, defined by the ratio of their input and output powers. In this operation regime, the amplifier is unable to compensate for losses in individual modes, but a constant total power profile is achieved [21]. We further consider the noise at the receiver to be spatially and spectrally white, leading to equal noise powers across all modes [14]. This condition becomes increasingly accurate for higher mode counts, longer distances, and wider bandwidths [25]. Based on these assumptions, we can define the SNR as the ratio between total signal optical power to the total optical noise power considering all supported modes

$$\text{SNR} = \frac{\sum_{i=1}^D \sigma_{u,i}^2}{D\sigma_\eta^2}, \quad (2)$$

where $\sigma_{u,i}^2$ is the i^{th} mode power and σ_η^2 is the per-mode noise power.

In practical systems, optical amplified spontaneous emission (ASE) is not the only source of AWGN. Transceiver imperfections, such as those generated at the analog-to-digital converter, also impose noise contributions that limit the system performance in scenarios of low ASE. Furthermore, the excess error generated in equalizers, particularly under the long differential mode delays encountered in SDM systems, also creates an additional noise contribution that affects the source separation process [14], [26], [27]. The SNR referenced in this paper pertains to an equivalent value at the input of the source separation process, achieved by a system free

of MDG. Such an approach is in line with [28], where the transceiver implementation penalty of transceivers can be measured beforehand in a back-to-back setup and modeled as an AWGN source.

The equivalent pre-filtering SNR is given by

$$\text{SNR} = \left(\frac{B_s}{12.5 \cdot 10^9 \cdot \text{GSNR}} + \frac{1}{\text{SNR}_{\text{imp}}} \right)^{-1}, \quad (3)$$

where GSNR is the measured generalized optical SNR in a 12.5 GHz bandwidth, and B_s is the signal bandwidth.

The SNR_{imp} is measured in a setup with no ASE noise or MDG, but with differential group delay (DGD) to account for the equalizer excess error generated, e.g., when its length is too short to compensate for the channel delay spread. The characterization of the excess error contribution for SNR_{imp} can be carried out by simulation or experimentally using the statistical models presented in [14]. It is important to emphasize that short links, where SNR_{imp} plays a more significant role, typically exhibit low delay spreads, resulting in minimal equalizer excess errors. On the other hand, in long SDM links, where the DGD is most pronounced, the contribution of SNR_{imp} becomes negligible because of intensive ASE accumulation.

B. Channel Power Gains Statistics

Assuming a linear MIMO AWGN channel, the linear scale eigenvalues λ_i of the $\mathbf{H}\mathbf{H}^H$ operator can be interpreted as power gains for the individual channels [29]. The eigenmodes obtained from the eigendecomposition operation are the Schmidt modes of the channel and represents an equivalent optimal basis of propagation [19]. The ratio between the signal power propagated along the i^{th} Schmidt mode and its respective noise power is given by $\lambda_i \cdot \text{SNR}$. The eigenvalues are sorted in ascending order ($\lambda_1 \leq \lambda_2 \leq \dots \leq \lambda_D$).

As pointed out in [13], the channel power gains in decibel units follow the well-defined fixed-trace GUE spectral probability density function (PDF). The unlabeled³ decibel power gain distribution is given by [13, Table 1], [14, Eq. (S.15)]

$$f_{\lambda_{\text{dB}}}(\lambda_{\text{dB}}) = \frac{\alpha_{\lambda_{\text{dB}},D}}{\sigma_{\text{mdg}}} e^{-\frac{(D+1)}{2} \left(\frac{\lambda_{\text{dB}} - \mu_{\lambda_{\text{dB}}}}{\sigma_{\text{mdg}}} \right)^2} \times \sum_{k=0}^{D-1} \beta_{\lambda_{\text{dB}},D,k} \left(\frac{\lambda_{\text{dB}} - \mu_{\lambda_{\text{dB}}}}{\sigma_{\text{mdg}}} \right)^{2k}, \quad (4)$$

where $\alpha_{\lambda_{\text{dB}},D}$ is a normalization factor, $\beta_{\lambda_{\text{dB}},D,k}$ are polynomial coefficients, $\mu_{\lambda_{\text{dB}}}$ is the average logarithmic gain such that the total linear power gain is unitary, and σ_{mdg} is the standard deviation of the unlabeled logarithmic eigenvalues, which is a common metric in literature to quantify the MDG. The coefficients of (4) are described in further detail in [13] and [30]. At the limit $D \rightarrow \infty$, (4) converges to the semicircular distribution presented in [13, Table 1], [15, I]

$$f_{\lambda_{\text{dB}}}(\lambda_{\text{dB}}) = \frac{1}{2\pi\sigma_{\text{mdg}}} \sqrt{4 - \frac{(\lambda_{\text{dB}} - \mu_{\lambda_{\text{dB}}})^2}{\sigma_{\text{mdg}}^2}}, \quad (5)$$

$$-2\sigma_{\text{mdg}} + \mu_{\lambda_{\text{dB}}} \leq \lambda_{\text{dB}} \leq 2\sigma_{\text{mdg}} + \mu_{\lambda_{\text{dB}}}.$$

³The unlabeled distribution considers the ensemble of all modal-gains λ regardless of index.

III. INFORMATION RATES IN MIMO SYSTEMS USING MMSE RECEIVERS

Optical SDM channels with MDG and random coupling exhibit channel gains λ_i that vary over time but preserve $\sum_{i=1}^D \mathbb{E}\{\lambda_i\} = D$. As a consequence, the average per-mode channel gain $\mathbb{E}\{\lambda\}$ is unitary. The information rate losses caused by MDG can be proven for any MDG distribution from Jensen's inequality, given that the logarithmic relation between capacity and SNR is concave [31]. Applying Jensen's inequality for concave functions to the Shannon's capacity formula yields

$$\mathbb{E}\{\log_2(1 + \lambda \cdot \text{SNR})\} \leq \log_2(1 + \mathbb{E}\{\lambda\} \text{SNR}), \quad (6)$$

As $\mathbb{E}\{\lambda\} = 1$, the expected per-mode capacity under MDG is, at most, equal to that of an equivalent single-mode link

$$\mathbb{E}\{\log_2(1 + \lambda \cdot \text{SNR})\} \leq \log_2(1 + \text{SNR}), \quad (7)$$

where the equality holds only if⁴ $\sigma_{\text{mdg}} = 0$ dB. This MDG impairment appears at the receiver as a SNR penalty [9].

A. Derivation of the post-MMSE filtering SINR

Several studies on the impact of MDG on the channel capacity assume an optimal ML receiver. However, coupled SDM systems using MMSE equalizers have further information rate losses because of co-channel interference [12]⁵. Therefore, the post-filtering SNR in a particular filter output is rather given by a SINR. The SINR in a particular filter output i relates to the channel matrix coefficients by [12, Eq. (9)]

$$\text{SINR}_i = \frac{1}{\left[(\mathbf{I} + \text{SNR} \cdot \mathbf{H}^H \mathbf{H})^{-1} \right]_{i,i}} - 1. \quad (8)$$

Equation (8) provides an instantaneous SINR_i for an instantaneous matrix realization \mathbf{H} . However, for some applications, such as calculating the average information rates in optical SDM systems, an average SINR_i is also desired. Until now, calculating the average SINR of signals affected by MDG after an MMSE equalizer has been accomplished by Monte-Carlo simulation of several realizations of \mathbf{H} . As the main contribution in this paper, we show in this section that an approximation for the average SINR in MDG-impaired signals can be analytically computed as

$$\text{SINR} = \left[\int_0^1 \frac{10 \cdot f_{\lambda_{\text{dB}}} \left(10 \cdot \log_{10} \left(\frac{1-x}{\text{SNR} \cdot x} \right) \right)}{\ln(10)(1-x)} dx \right]^{-1} - 1. \quad (9)$$

The expression is analytically exact at the limiting case of $D \rightarrow \infty$ ⁶. The full derivation is presented in [appendix A](#).

⁴ $\mathbb{E}\{f(X)\} = f(\mathbb{E}\{X\})$ only holds if $f(\cdot)$ is affine or $\sigma_X = 0$. This is a known result of functional inequalities [32]. As the logarithmic relation between capacity and SNR is strictly concave, only the latter case provides the equality.

⁵In MIMO MMSE equalizers parallel data streams generate co-channel interference. More sophisticated equalization techniques, such as successive interference cancellation (SIC) equalization, approach the performance of ideal ML filtering [33].

⁶Throughout the rest of the paper, variable SINR, without index, represents this exact solution.

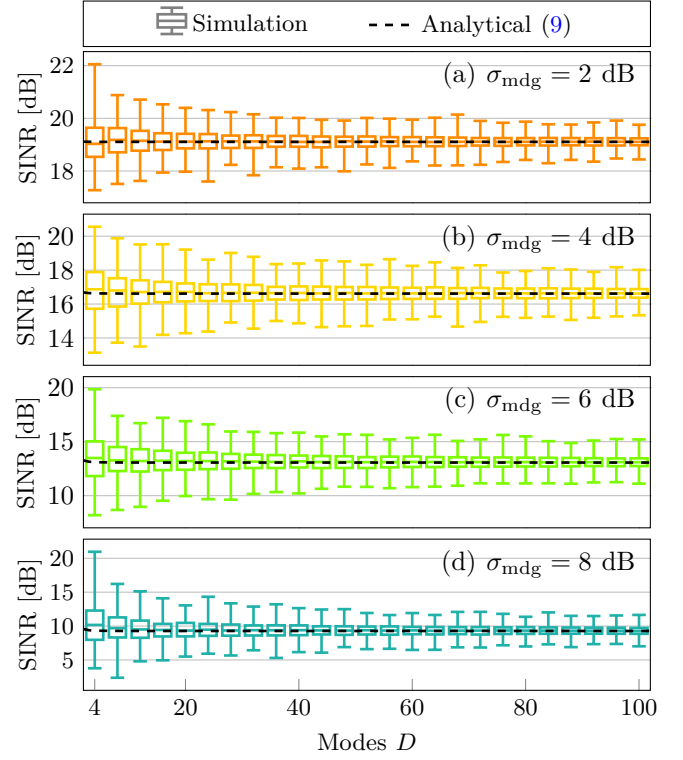


Fig. 1: Box plots of the SINR simulated values compared to the analytical solution with respect to the mode-count for $\text{SNR} = 20$ dB. The simulations rely on the parameters given in Table I, with a modification on the frequency bin count (to 1 frequency bin) for no frequency diversity. The simulated distribution considers all modes regardless of the index.

In the limiting case of $D \rightarrow \infty$, as the standard deviation of the per-mode gains scales by $1/D$ [30, Eq. (6)], the λ_i values converge to deterministic solutions and the SINR of all modes approach (9). This effect of reduced variance due to increased mode diversity has been previously discussed in [34], [35].

Under finite mode counts, the solution given in (9) can be used as an approximation for the average SINR, as

$$\mathbb{E} \left\{ \sum_{i=1}^D \frac{1}{D} \text{SINR}_i \right\} \approx \text{SINR}. \quad (10)$$

Fig. 1 shows box plots for the post-equalization SINR, obtained by simulation. The parameters used in all simulations are given in Table I, unless explicitly stated otherwise. To generate Fig. 1, the channel coefficients λ_i are randomly simulated and evaluated through matrix operations. The simulated channel matrices are generated using the multi-section model⁷ presented in [13, Eq. (2)]. The impact of fiber attenuation appears as a reduced SNR at the end of the link. The simulations for Fig. 1 consider a worst-case scenario of only 1 frequency bin, as frequency diversity reduces the variance of information rate metrics [36]. Fig. 1 reveals a good agreement between the simulated average SINR and the results generated by the

⁷The multi-section model accounts for random modal coupling and MDG, neglecting nonlinearities.

Parameter	Value
Monte-Carlo trials per point	20
Supported modes	6 (3 spatial modes \times 2 polarizations)
Number of frequency bins	1000
Chromatic dispersion	22 ps/nm/km
Per-section DGD	3.1 ps/ $\sqrt{\text{km}}$
Number of sections	100
Section length	50 km
Carrier Frequency	1550 nm
Symbol rate	30 GBaud
Time domain channel granularity	8 samples/symbol
RX oversampling rate	2 samples/symbol
Equalizer taps	1000
Training symbols	$8 \cdot 10^5$
Total number of symbols	$10 \cdot 10^5$

TABLE I: Simulation parameters used for Monte-Carlo simulations for a single frequency channel.

analytical formula, with the SINR variance decreasing towards higher mode counts owing to mode diversity.

To assess the approximation in (10), we compare the analytical solution with simulations of a 3-mode polarization multiplexed link ($D = 6$), which is the lowest mode count supported in FMFs, resulting in the highest divergences to (9) because of low mode diversity. The simulation and analytical curves of average SINR are presented in Fig. 2(a). The results reveal that (9) is a valid approximation for practical values of MDG ($\sigma_{\text{mdg}} < 10$ dB) even for low mode counts. At high SNR and high MDG values, the analytical curve underestimates the average SINR by a small margin.

A more tangible metric to express the impact of MDG on the system performance is the effective SNR loss, defined as [9, Eq. (14)]

$$\Delta_{\text{mmse}} = 10 \cdot \log_{10}(\text{SNR}) - 10 \cdot \log_{10}(\text{SINR}). \quad (11)$$

Fig. 2(b) demonstrates severe losses caused by MDG, resulting in several decibels of penalty. In some cases, the MDG-induced penalties can nullify any benefits of low AWGN setups. However, practical systems should not be allowed to operate under such extreme MDG conditions. In any case, the analytical model reveals a suitable accuracy in predicting effective SNR losses, particularly for $\sigma_{\text{mdg}} < 10$ dB.

B. Capacity

In the previous section, we derived an analytical expression for the signal SINR after MMSE filtering. In this section, we apply (9) to the Shannon formula to calculate the capacity of MIMO channels incorporating MMSE equalizers. The average per-mode capacity with MMSE equalization and non-zero MDG, under the AWGN channel model, in bits/s/Hz/mode, is given by

$$C_{\text{mmse}} = \frac{1}{D} \sum_{i=1}^D \log_2(1 + \text{SINR}_i). \quad (12)$$

As previously discussed, we use the limiting case of an infinite number of modes to derive an approximation for the

average SINR, yielding a limiting value for the per-mode capacity

$$C_{\text{mmse}} \approx \lim_{D \rightarrow \infty} \frac{1}{D} \sum_{i=1}^D \log_2(1 + \text{SINR}_i) = \log_2(1 + \text{SINR}). \quad (13)$$

Fig. 3(a) compares analytical and simulation values, for C under both ideal ML equalization and MMSE equalization. Both capacity values are severely impaired by MDG, with setups applying MMSE filtering suffering a higher penalty. The curves reveal excellent agreement between simulation and the analytical model.

As discussed in [9], capacity loss metrics are also relevant to express the penalties caused by MDG. The capacity loss metric defined in [9] is given by

$$\xi = 1 - \frac{C_{\text{mmse}}}{C_{\text{awgn}}}, \quad (14)$$

where C_{awgn} is the average per-mode capacity of an equivalent link with only AWGN and without MDG. In the scope of this paper, C_{awgn} is defined as

$$C_{\text{awgn}} = \frac{1}{D} \sum_{i=1}^D \log_2(1 + \text{SNR}) = \log_2(1 + \text{SNR}). \quad (15)$$

The capacity loss evaluated for simulations, and for the analytical model is shown in Fig. 3(b), as a function of MDG. As discussed in previous papers, there is a significant capacity reduction if MDG is left unmanaged. These penalties are especially relevant with MMSE equalization. The MDG impact can become so significant that the capacity of the spatially multiplexed system can become equivalent to that of a single standard single-mode fiber (SSMF), eliminating all the benefits of SDM.

Fig. 3 also relates capacity metrics to the span count [13], highlighting the analytical model as a powerful design tool. The relationship is carried out assuming an optical link with homogeneous spans with constant per-section MDG standard deviation (σ_g). The approximate formula provided in [13, Eq. (1)], which is accurate for σ_{mdg} values up to 10 dB, enables to relate σ_{mdg} and distance for selected per-section σ_g values. Such transparent reach analysis has been discussed in greater detail in [9] and [35]. Fig. 3 confirms the large impact of minimal changes in per-section MDG values on capacity in long-haul terrestrial and submarine links with high accumulated MDG [37]–[39].

Due to the stochastic nature of MDG, variations in information rate are expected and can result in outages. For non-infinite mode-count links, the SINR is a stochastic value as seen in Fig. 1, and the calculation of such variance is still an open problem. For optimal ML equalization, analytical models for the capacity variance are provided in [30].

C. Pre-FEC BER and Constrained Capacity

Complementing the previous section on capacity evaluation, this section investigates the performance of the proposed analytical model in predicting the pre-FEC BER and constrained

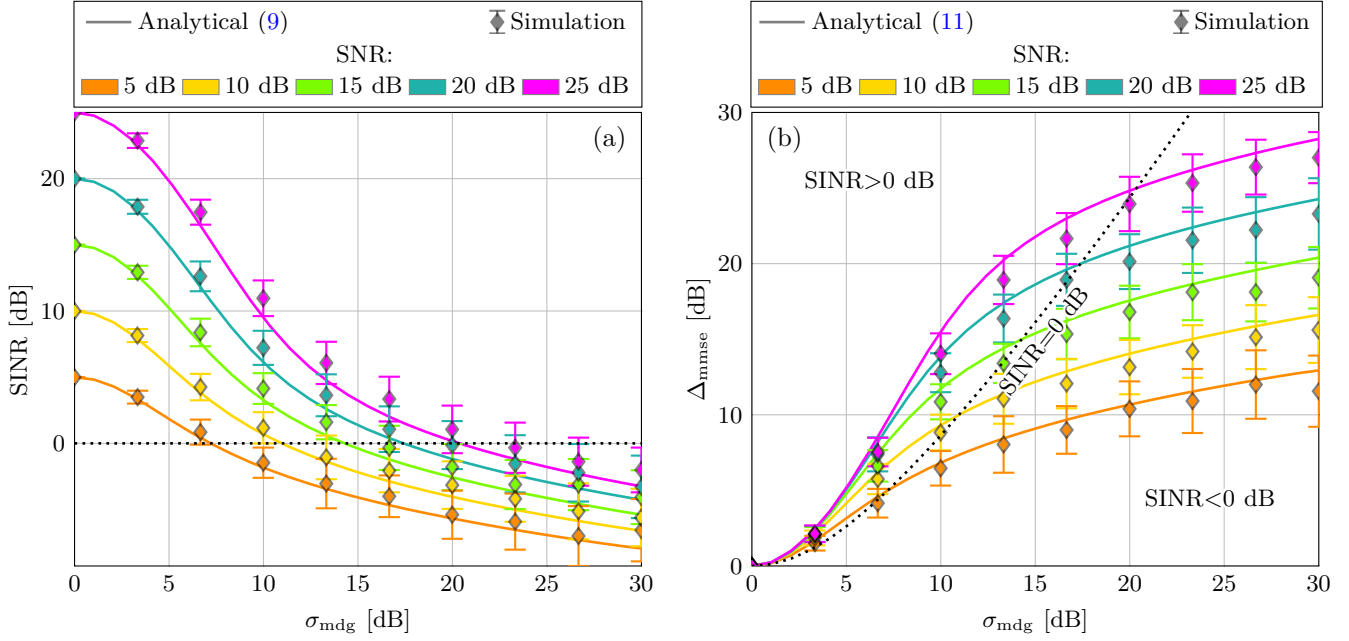


Fig. 2: (a) Average SINR as a function of σ_{mdg} for $D = 6$. (b) Effective SNR loss due to MDG as a function of σ_{mdg} for $D = 6$. The 0 dB SINR line in (b) is obtained from the σ_{mdg} values where $\Delta_{\text{mmse}} = 10 \cdot \log_{10}(\text{SNR})$. The curves obtained from Monte-Carlo simulation are presented alongside the analytical predictions. The markers show the simulation sample mean, and error bars correspond to one sample standard deviation.

capacity considering particular modulation formats. In a M -QAM modulated transmission scheme with Gray mapping, the SINR relates to the pre-FEC BER by [40, Eq. (6.20)]

$$b_e \approx \frac{2(M-1)}{M \log_2(M)} Q \left(\sqrt{\frac{6}{M^2-1}} \text{SINR} \right), \quad (16)$$

where $Q(\cdot)$ is the Q-function.

In addition to the pre-FEC BER, the constrained capacity, given in bits per symbol, is also a relevant metric to incorporate rate limitations imposed by modulation [42]. The constrained capacity, or mutual information (MI), corresponding to a M -QAM sequence, can be obtained by the J -point Gauss-Hermite quadrature approximation given by [43, Eq. (40)]

$$I \approx \log_2(M) - \frac{1}{M\pi} \sum_{(i,l_1,l_2)=(1,1,1)}^{(M,J,J)} w_{l_1} w_{l_2} \times \log_2 \sum_{j=1}^M e^{-\text{SINR} \cdot \|\mathbf{d}_{i,j}\|^2 + 2\sqrt{\text{SINR}} \cdot \mathbb{R}\{(\chi_{l_1} \hat{\mathbf{i}} + \chi_{l_2} \hat{\mathbf{j}}) \cdot \mathbf{d}_{i,j}\}} \quad (17)$$

where $\mathbf{d}_{i,j}$ is the distance vector between the i^{th} and j^{th} unitary power constellation coordinates, $\|\cdot\|$ is the Euclidean norm, $\mathbb{R}\{\cdot\}$ is the real part, \cdot is the dot product, and χ_k and w_k are, respectively, the Gauss-Hermite quadrature nodes and weights, given for $J = 5$ and $J = 10$ in [44, Table 3.5.10 and Table 3.5.11].

Figs. 4(a-b) show the impact of MDG on the average total pre-FEC BER and on the MI, respectively. We compare the analytical solutions given in (16) and (17), with end-to-end simulations of a complete SDM systems. In comparison with the previous simulations, which only simulate random channel

matrices, we now consider the generation of random symbol sequences, their propagation along a randomly coupled channel, and the recovery processes at the receiver. In addition to the curves, we show the equivalent transparent reach distance as a function of MDG. As noted for the SINR, the information rate is overestimated at high SNR and MDG values. These curves confirm the applicability of the derived analytical model to the design of practical SDM systems.

As we discussed earlier, the analysis is based on averages. Under practical scenarios, a certain operational margin is required to address the probability of outages. Nevertheless, as discussed in [34] and [36], modal and frequency diversity induces an averaging effect that largely reduces the stochastic variation of capacity metrics.

IV. PERFORMANCE MONITORING

This section addresses the task of performance monitoring in SDM receivers using information available in MMSE equalizers. In particular, two metrics are estimated: the accumulated link MDG and the pre-equalizer SNR. Indeed, although estimating the SNR is trivial in traditional polarization-multiplexed receivers, this task is complicated in SDM systems because of the performance losses generated by MDG. Aligned with previous works [45]–[51], we also use the MMSE equalizer coefficients as inputs for the proposed estimation technique. In [45], [46], we derive an analytical solution for σ_{mdg} estimation based on a correction factor applied to the standard deviation of the equalizer inverse eigenvalues. However, the proposed technique shows limitations under high-MDG and low-SNR due to the multivalued behavior of the equalizer inverse eigenvalues. In [47], we propose a

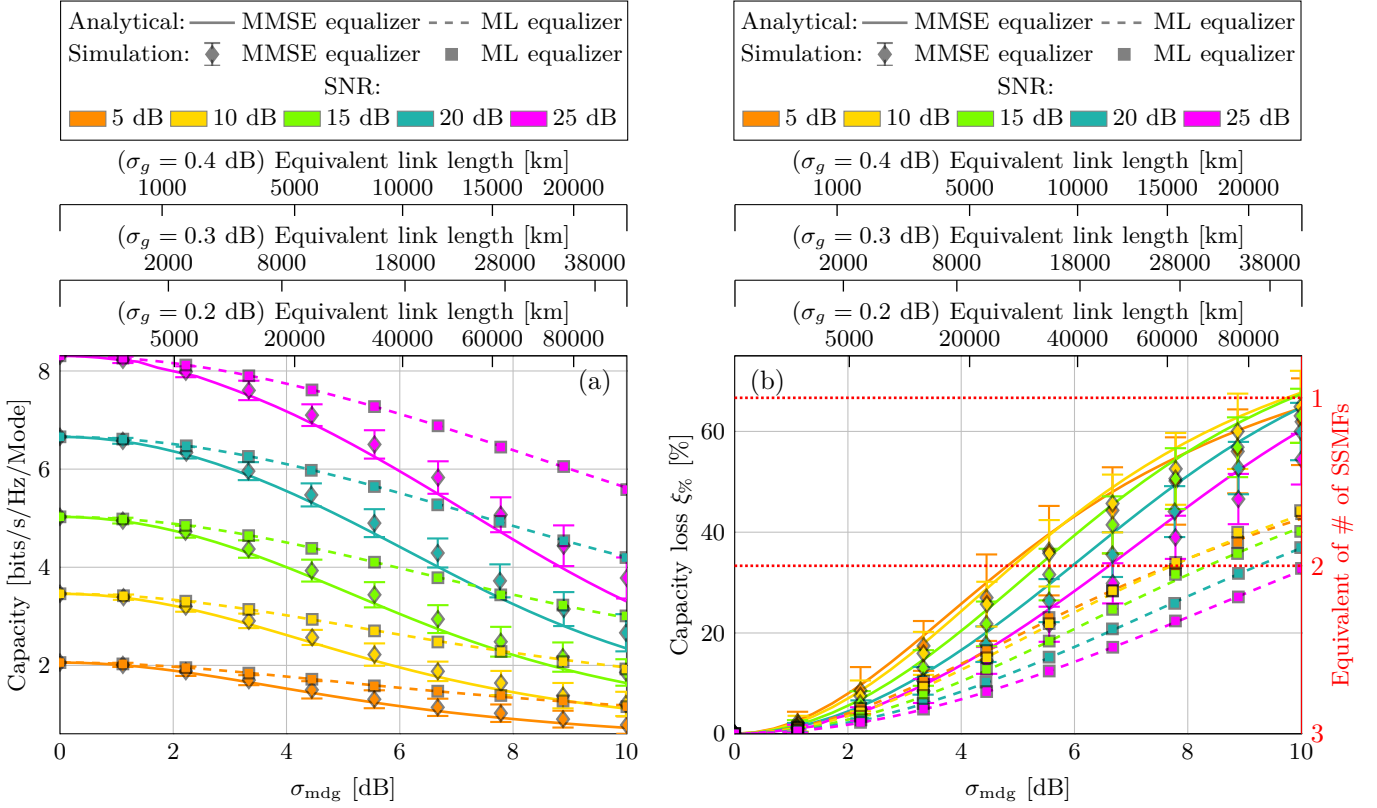


Fig. 3: (a) Average capacity curves as a function of σ_{mdg} for $D = 6$. (b) Capacity loss due to MDG as a function of σ_{mdg} for $D = 6$. The MMSE equalizer analytical curves are derived from (13), whereas the ideal ML equalizer curves are derived from [13, Eq. (10)]. The curves obtained from Monte-Carlo simulations are presented alongside the analytical predictions. The markers show the simulation sample mean, and error bars correspond to one sample standard deviation. In (b) it is shown, for comparison, the number of SSIMFs that yield equivalent capacity. We also present the equivalent transparent reach as a function of σ_{mdg} for selected per-section MDG (σ_g) values, considering a 50-km section length.

neural-network-based technique for σ_{mdg} and SNR estimation, discussed in further detail in [49]. In [51], a similar neural network approach was proposed for capacity loss estimation. All these techniques are validated experimentally demonstrating significant accuracy. This section leverages our recent results on MMSE equalizers to derive a look-up-table-based solution for the pre-filtering SNR and σ_{mdg} estimation with suitable accuracy for a wide range of values.

A. Statistics of the MIMO MMSE equalizer

As the MIMO MMSE equalizer matrix \mathbf{W} coincides with the zero-forcing solution \mathbf{H}^{-1} in noise-free scenarios, the equivalent matrix product $\mathbf{W}^{-1}(\mathbf{W}^{-1})^H$ is often used for parameter estimation [45]–[50]. The logarithmic scale MIMO MMSE eigenvalues $\lambda_{\text{dB},i}^{\mathbf{W}}$, are related to the logarithmic scale power gains $\lambda_{\text{dB},i}$, by [45, Eq. (3)]

$$\lambda_{\text{dB},i}^{\mathbf{W}} = 20 \cdot \log_{10} \left(\frac{1}{\text{SNR}} 10^{\frac{-\lambda_{\text{dB},i}}{10}} + 1 \right) + \lambda_{\text{dB},i}. \quad (18)$$

Fig. 5 illustrates (18) for a wide range of SNR values. In (18) there is an inflection point at $-10 \cdot \log_{10}(\text{SNR})$. For channel eigenvalues below $\lambda_i < \text{SNR}^{-1}$, the linear scale equalizer inverse eigenvalues ($\lambda_i^{\mathbf{W}}$) is multivalued, impairing parameter estimation techniques [45], [46], [50].

From (18), via transformation, we obtain the following relation between the PDFs of then logarithmic-scale eigenvalues λ_{dB} from the channel and the equalizer

$$f_{\lambda_{\text{dB}}^{\mathbf{W}}}(\lambda_{\text{dB}}^{\mathbf{W}}) = \frac{f_{\lambda_{\text{dB}}} (g^{\oplus}(\lambda_{\text{dB}}^{\mathbf{W}})) + f_{\lambda_{\text{dB}}} (g^{\ominus}(\lambda_{\text{dB}}^{\mathbf{W}}))}{\sqrt{1 - \frac{4}{\text{SNR}} \cdot 10^{\frac{-\lambda_{\text{dB}}^{\mathbf{W}}}{10}}}}, \quad (19)$$

$$\lambda_{\text{dB}}^{\mathbf{W}} > 10 \cdot \log_{10} \left(\frac{4}{\text{SNR}} \right),$$

where $g^{\oplus}(\cdot)$ and $g^{\ominus}(\cdot)$ are, respectively, the positive and negative root solutions of

$$g(\lambda_{\text{dB}}^{\mathbf{W}}) = 10 \cdot \log_{10} \left[-\text{SNR}^{-1} + \frac{1}{2} 10^{\frac{\lambda_{\text{dB}}^{\mathbf{W}}}{10}} \right. \\ \left. \times \left(1 \pm \sqrt{1 - \frac{4}{\text{SNR}} \cdot 10^{\frac{-\lambda_{\text{dB}}^{\mathbf{W}}}{10}}} \right) \right]. \quad (20)$$

The mean and standard deviation of the equalizer eigenvalues can be obtained via numeric integration of (19).

Fig. 6 shows the relation between the standard deviation of the unlabeled eigenvalues derived from the channel matrix (σ_{mdg}) and those derived from the equalizer inverse (σ_{mmse}). Real and estimated values start to significantly deviate in the

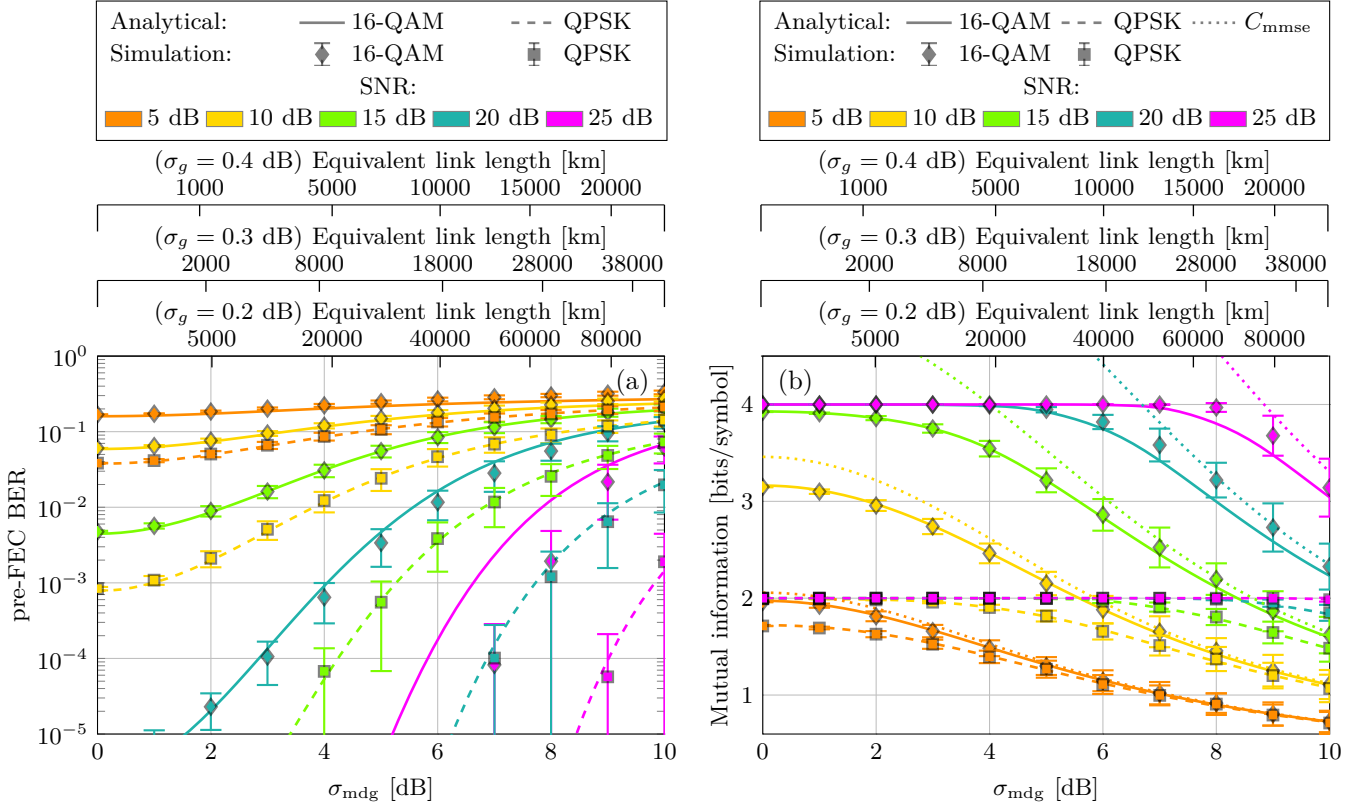


Fig. 4: (a) Average pre-FEC BER as a function of σ_{mdg} for $D = 6$. (b) MI as a function of σ_{mdg} for $D = 6$. The pre-FEC BER is obtained from (16), whereas the MI is obtained from (17) considering a 10-point Gauss-Hermite quadrature. The curves obtained from Monte-Carlo simulations are presented alongside the analytical results. The markers show the simulation sample mean, and error bars correspond to one sample standard deviation. The simulation considers the transmitter and receiver as given by Table I, whereas the BER is obtained from the post-decision binary sequence and the MI is derived from the post-filtering symbol sequence for an AWGN channel, by the method described in [41]. In (b), we show the capacity alongside the mutual information obtained from (13). We also present the equivalent transparent reach as a function of σ_{mdg} for selected per-section MDG (σ_g) values, considering a 50-km section length.

vicinity of the inflection point of (18). From the boundaries of the limiting case given in (5), the equalizer inverse will have an approximate linear relation to the channel with sufficiently high SNR if

$$-2\sigma_{\text{mdg}} + \mu_{\lambda_{\text{dB}}} \gg -10 \cdot \log_{10}(\text{SNR}). \quad (21)$$

While we discussed before the asymptotic behavior of \mathbf{W}^{-1} approaching \mathbf{H} as SNR tends to infinity, (21) provides a rule of thumb for which the approximation $\mathbf{W}^{-1} \approx \mathbf{H}$ can be considered accurate for MDG estimation. Fig. 6 visually illustrates how real and estimated eigenvalues (solid and dotted curves) deviate near the limit given by vertical dashed lines.

Applying (4) to (19) enables us to obtain the unlabeled $\lambda_{\text{dB}}^{\mathbf{W}}$ distribution. As detailed in [30, Section III], the per-mode logarithmic gain PDF can be well approximated by a Gaussian distribution with mean $\mu_{\lambda_{\text{dB},i}}$ and standard deviation $\sigma_{\lambda_{\text{dB},i}}$. The per-mode $\lambda_{\text{dB},i}^{\mathbf{W}}$ PDF, in turn, can be obtained from the per-mode $\lambda_{\text{dB},i}$ PDF $f_{\lambda_{\text{dB},i}}(\lambda_{\text{dB},i})$ given by the approximate analytical solution in [30, Eq. (7)].

B. Estimation of the pre-filtering SNR and MDG

The σ_{mmse} and SINR are metrics can be readily estimated by receiver digital signal processing (DSP). The SINR can be estimated using the error vector magnitude of the post-equalizer constellations. The σ_{mmse} can be estimated from the frequency domain equalizer inverse matrix. If the equalizer operates in the time domain, a discrete Fourier transform algorithm is required. Considering a discrete-time frequency domain equalizer $\mathbf{W}[\omega]$, $\omega \in [1, \Omega]$, where Ω is the equalizer discrete frequency bin count, σ_{mmse} can be estimated from

$$\hat{\sigma}_{\text{mmse}}^2 = \sum_{(\omega,i)=(1,1)}^{(\Omega,D)} \frac{\left[\text{eig}_i \left(\mathbf{W}^{-1}[\omega] (\mathbf{W}^{-1}[\omega])^H \right) - \mu_{\text{mmse}} \right]^2}{\Omega \cdot D - 1}, \quad (22)$$

where $\text{eig}_i(\cdot)$ return the i^{th} ordered eigenvalue, and μ_{mmse} is the average of the equalizer inverse unlabeled eigenvalues, estimated from

$$\mu_{\text{mmse}} = \sum_{(\omega,i)=(1,1)}^{(\Omega,D)} \frac{\text{eig}_i \left(\mathbf{W}^{-1}[\omega] (\mathbf{W}^{-1}[\omega])^H \right)}{\Omega \cdot D}. \quad (23)$$

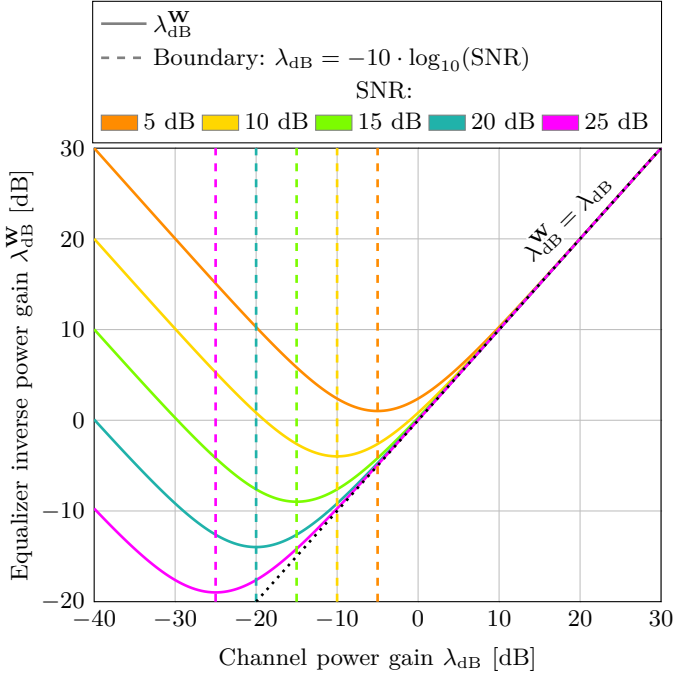


Fig. 5: Relation between the channel logarithmic power gain, obtained from the eigenvalues of the channel matrix, and the equalizer inverse logarithmic power gain, obtained from the equalizer inverse matrix [45].

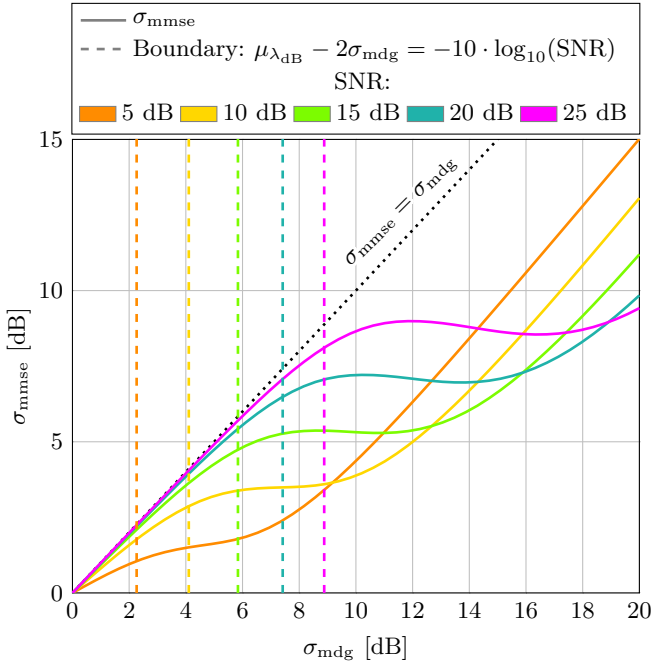


Fig. 6: Relation between the standard deviation of the equalizer inverse logarithmic power gain (σ_{mmse}) and the standard deviation of the channel logarithmic power gain (σ_{mdg}) for $D = 6$. The boundaries given by (21) are also presented. The σ_{mmse} is obtained via numeric integration of (19).

Interestingly, any unique SNR and σ_{mdg} pair within a practical range of values yields a unique SINR and σ_{mmse}

pair (shown numerically in appendix B). While a closed-form analytical equation relating SNR and σ_{mdg} as functions of SINR and σ_{mmse} is unknown, it is possible to obtain this relation by numerically inverting the direct equation. Considering $\widehat{\text{SINR}}$ and $\widehat{\sigma}_{\text{mmse}}$ as measured parameters, we calculate SNR and $\widehat{\sigma}_{\text{mdg}}$ by minimizing the squared error to their analytical equivalents, i.e.,

$$(\widehat{\text{SNR}}, \widehat{\sigma}_{\text{mdg}}) = \underset{\text{SNR}, \sigma_{\text{mdg}}}{\text{argmin}} \left(\mathbb{E} \left\{ [\widehat{\sigma}_{\text{mmse}} - \sigma_{\text{mmse}}]^2 \right\} + \mathbb{E} \left\{ [\widehat{\text{SINR}} - \text{SINR}]^2 \right\} \right), \quad (24)$$

where SINR and σ_{mmse} are obtained analytically from (9) and (19) respectively.

The estimation process given in (24) can be performed iteratively, until a minimum error or iteration threshold is reached. Alternatively, given that the method relies on a numeric process, for fast real-time estimation, precomputed values can be stored in a look-up table (LUT) with sufficient granularity.

Fig. 7 shows the σ_{mdg} and SNR estimation error from simulated values considering a complete SDM link transmission, with parameters as given by Table I, and using a pre-computed LUT. The used LUT sweeps the SNR for 100 logarithmic-spaced points from 0 to 30 dB, and the σ_{mdg} for 100 points from 0 to 20 dB. Fig 7(a) confirms accurate σ_{mdg} estimation for the entire evaluated range, with some divergence at the lowest and highest SNR values. Fig 7(b) shows discrepant values at high SNR values, but accurate estimations for the rest of the evaluated region. The estimation error at high SNR can be attributed to the previously mentioned underestimation of the analytical SINR within this region. In any case, practical scenarios with high SNR and high MDG are rare, as both effects accumulate with cascaded spans. From the estimated SNR and σ_{mdg} values, additional meaningful performance metrics can be calculated, such as the MDG-induced capacity loss or effective SNR loss [9].

V. CONCLUSION

We derive analytical expressions to quantify the effects of MDG in strongly-coupled SDM systems with MIMO MMSE equalization, including a closed-form expression for the system information rate. The presented solutions describe with suitable accuracy the average behavior of such systems within practical values of SNR and MDG. The provided solutions enable fast system analysis, avoiding the use of costly semi-analytical simulations for average capacity evaluation. Furthermore, we review the statistical behavior of the MIMO MMSE equalizer coefficients under strongly-coupled SDM systems. We show a practical region where the MIMO MMSE equalizer inverse can be utilized as an approximation to the channel. We also demonstrate that the mapping between relevant parameters before and after the MMSE equalizer are single-valued, enabling a look-up-table based method for performance monitoring.

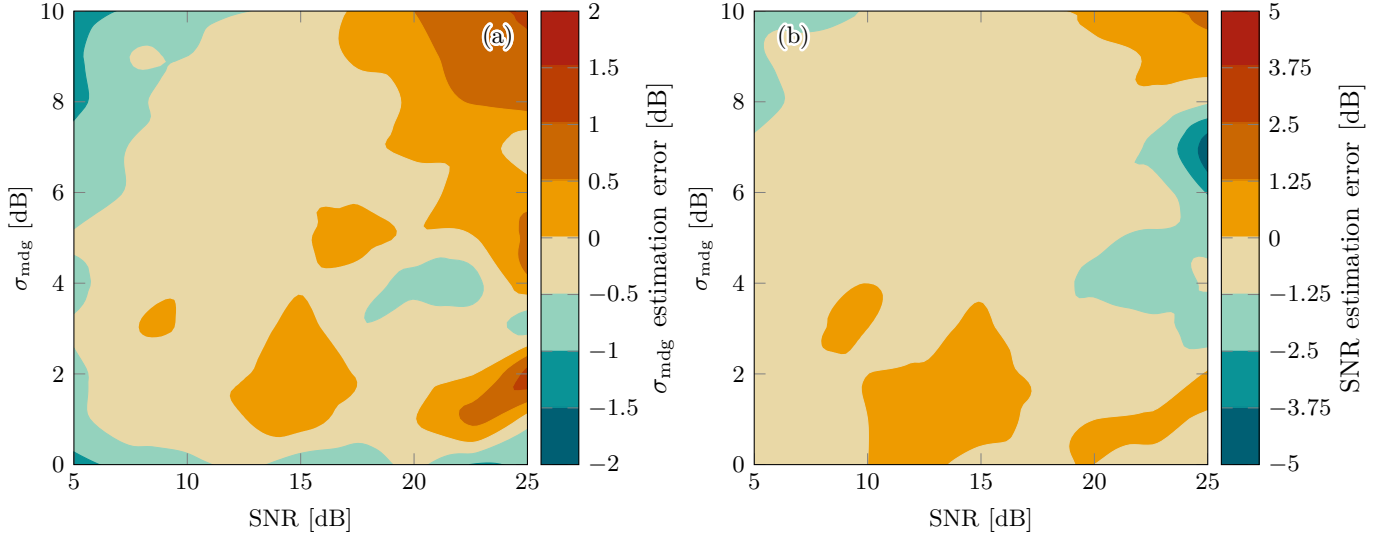


Fig. 7: Parameter estimation error for σ_{mdg} (a) and for SNR (b) from (24). The estimation technique utilizes a LUT, where the measured SINR and σ_{mmse} are compared against pre-calculated analytical results. Each estimated value is obtained from the average of 10 uncorrelated SINR and σ_{mmse} samples from a simulated setup with QPSK modulated symbol sequence.

APPENDIX A

ANALYTICAL SOLUTION FOR THE AVERAGE SINR OF A SYSTEM WITH MDG AND USING AN MMSE EQUALIZER

Considering the eigenvector matrix \mathbf{Q} and the eigenvalue diagonal matrix $\mathbf{\Lambda}$ from the eigendecomposition of $\mathbf{H}^H \mathbf{H}$, we can rewrite (8) as

$$\begin{aligned} \text{SINR}_i &= \frac{1}{\left[(\mathbf{Q} \mathbf{Q}^{-1} + \text{SNR} \cdot \mathbf{Q} \mathbf{\Lambda} \mathbf{Q}^{-1})^{-1} \right]_{i,i}} - 1 \\ &= \frac{1}{\left[\mathbf{Q} (\mathbf{I} + \text{SNR} \cdot \mathbf{\Lambda})^{-1} \mathbf{Q}^{-1} \right]_{i,i}} - 1. \end{aligned} \quad (25)$$

The eigenvalues $\mathbf{\Lambda}$ are the same values as obtained from the eigendecomposition of $\mathbf{H} \mathbf{H}^H$, given that the channel matrix is square. However, the eigenvectors have distinct values. Nevertheless, $\mathbf{H}^H \mathbf{H}$ is also a valid GUE matrix in a logarithmic scale.

The eigenvector matrix \mathbf{Q} is given by

$$\mathbf{Q} = \begin{bmatrix} v_{1,1} & v_{2,1} & \cdots & v_{D,1} \\ v_{1,2} & v_{2,2} & \cdots & v_{D,2} \\ \vdots & \vdots & \ddots & \vdots \\ v_{1,D} & v_{2,D} & \cdots & v_{D,D} \end{bmatrix}, \quad (26)$$

where $v_{i,j}$ is the j^{th} element of the eigenvector \mathbf{v}_i . Given that $\mathbf{Q}^{-1} = \mathbf{Q}^H$, the element (i, i) of the denominator of (25) can be simplified to scalar operations of the eigenvector elements

$$\text{SINR}_i = \left[\sum_{j=1}^D |v_{i,j}|^2 (1 + \text{SNR} \cdot \lambda_j)^{-1} \right]^{-1} - 1. \quad (27)$$

The eigenvector ensemble is uniformly distributed along the set of unitary norm vectors [18], [52]. For any eigenvector

\mathbf{v}_i , its elements are distributed such that the norm is unitary, resulting in the following joint PDF

$$f_{\mathbf{v}_i}(\mathbf{v}_i) = \alpha_{\mathbf{v}_i, D} \delta \left(1 - \sum_{j=1}^D |v_{i,j}|^2 \right), \quad 0 \leq |v_{i,j}|^2 \leq 1, \quad (28)$$

where $\delta(\cdot)$ is the Kronecker delta, and $\alpha_{\mathbf{v}_i, D}$ is a normalization factor obtained from the surface area of the D^{th} dimensional unit sphere

$$\alpha_{\mathbf{v}_i, D}^{-1} = \frac{2^{1-D} \pi^{\frac{D}{2}}}{\Gamma(\frac{D}{2})}, \quad (29)$$

where $\Gamma(\cdot)$ is the gamma function.

Each eigenvector element squared modulus has the following distribution [53]

$$f_{|v_{i,j}|^2}(|v_{i,j}|^2) = (D-1)(1-|v_{i,j}|^2)^{D-2}, \quad (30)$$

with mean

$$\mathbb{E}\{|v_{i,j}|^2\} = \frac{1}{D}. \quad (31)$$

We can rewrite the term inside the brackets in (27) as

$$\text{SINR}_i = \left[D \sum_{j=1}^D \frac{1}{D} |v_{i,j}|^2 (1 + \text{SNR} \cdot \lambda_j)^{-1} \right]^{-1} - 1, \quad (32)$$

where the summation in respect to j is a sample mean. The sample mean converges to the expectation as D approaches infinity

$$\lim_{D \rightarrow \infty} \text{SINR}_i = \lim_{D \rightarrow \infty} \left[D \cdot \mathbb{E} \left\{ |v_{i,j}|^2 (1 + \text{SNR} \cdot \lambda)^{-1} \right\} \right]^{-1} - 1. \quad (33)$$

We omit j of λ to avoid confusion, as the expectation of the marginal eigenvalues is not equal to that of the unlabeled distribution due to the previously defined eigenvalue ordering. Expectation is carried out over the set of eigenvector elements \mathbf{v}_i and the set of eigenvalues λ . As the GUE is invariant

under unitary transformations [18], [54], the eigenvectors and eigenvalues are uncorrelated. Therefore, we can split the expectation terms as

$$\lim_{D \rightarrow \infty} \text{SINR}_i = \lim_{D \rightarrow \infty} \left[D \cdot \mathbb{E} \{ |v_{i,j}|^2 \} \mathbb{E} \left\{ (1 + \text{SNR} \cdot \lambda)^{-1} \right\} \right]^{-1} - 1. \quad (34)$$

We can finally simplify the equation with (31) and omit the SINR index, as

$$\lim_{D \rightarrow \infty} \text{SINR} = \left[\mathbb{E} \left\{ (1 + \text{SNR} \cdot \lambda)^{-1} \right\} \right]^{-1} - 1. \quad (35)$$

Using random variable transformation, and expanding the expectation operator, yields

$$\text{SINR} = \left[\int_{x_0}^{x_f} \frac{10 \cdot f_{\lambda_{\text{dB}}} \left(10 \cdot \log_{10} \left(\frac{1-x}{\text{SNR} \cdot x} \right) \right)}{\ln(10)(1-x)} dx \right]^{-1} - 1. \quad (36)$$

where the integration limits x_0 and x_f are restricted by the term inside the logarithm

$$\frac{1-x}{\text{SNR} \cdot x} > 0, \quad (37)$$

resulting in

$$0 < x < 1. \quad (38)$$

Replacing the limits in (36) we obtain (9).

APPENDIX B PROOF OF $(\text{SINR}, \sigma_{\text{mmse}})$ AND $(\text{SNR}, \sigma_{\text{mdg}})$ SINGLE-VALUEDNESS

The inverse function theorem states that any continuously differentiable function will be invertible in a region around a certain point if the Jacobian determinant at that point is non-zero [55]. For our purposes, the invertibility of a $(\text{SINR}, \sigma_{\text{mmse}})$ pair as a function of a $(\text{SNR}, \sigma_{\text{mdg}})$ pair, within a region of interest, guarantees that there is a unique single-valued mapping between both pairs.

The values of SINR and σ_{mmse} are smooth functions for all SNR and σ_{mdg} values of interest ($\text{SNR} > 0$ dB and $\sigma_{\text{mdg}} > 0$ dB). The SINR is monotonic decreasing in respect to σ_{mdg} and increasing in respect to SNR within the region of interest. As σ_{mmse} is a standard deviation value, it is real, finite, and non-negative for any valid $f_{\lambda_{\text{dB}}}(\lambda_{\text{dB}}^{\text{W}})$ PDF.

The Jacobian matrix for SINR and σ_{mmse} is given by

$$\mathbf{J} = \begin{bmatrix} \frac{\partial \text{SINR}}{\partial \text{SNR}} & \frac{\partial \text{SINR}}{\partial \sigma_{\text{mdg}}} \\ \frac{\partial \sigma_{\text{mmse}}}{\partial \text{SNR}} & \frac{\partial \sigma_{\text{mmse}}}{\partial \sigma_{\text{mdg}}} \end{bmatrix} \quad (39)$$

Obtaining a closed-form solution for (39) is not trivial. However, it can be solved numerically within a desired range. In Fig. 8, we evaluate the Jacobian determinant along a wide range of values ($\text{SNR} \in (0, 30)$ dB, $\sigma_{\text{mdg}} \in (0, 20)$ dB). We evaluate both SNR and SINR in logarithmic scale, as it is a monotonic function that preserves single-valuedness while keeping the unit scale within practical ranges. Fig. 8 shows that, with the asymptotic exception of $\text{SNR} \rightarrow 0$ dB and $\sigma_{\text{mdg}} \rightarrow 0$ dB, $|\mathbf{J}|$ is never zero. Therefore, any $(\text{SINR}, \sigma_{\text{mmse}})$

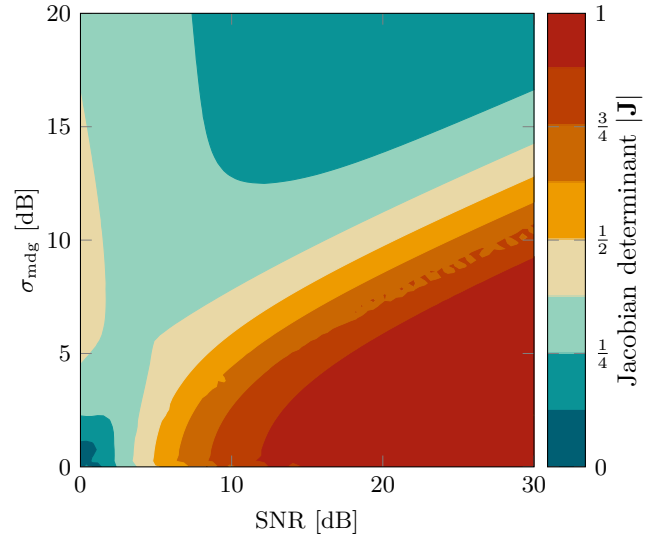


Fig. 8: Jacobian determinant of $(\text{SINR}, \sigma_{\text{mmse}})$ with respect to $(\text{SNR}, \sigma_{\text{mdg}})$. The solutions were obtained numerically, from the analytical solutions for the limiting case ($D \rightarrow \infty$).

pair values is related to a single unique $(\text{SNR}, \sigma_{\text{mdg}})$ pair within the evaluated region.

The Jacobian determinant also provides a measure of the intensity of correlation between sets, i.e. how a fixed deviation along the input variables propagates to the outputs. The greater the absolute Jacobian determinant, the greater the propagated deviation. Fig. 8 shows that the highest absolute Jacobian determinant, and therefore, the higher correlation between the measured and desired variables, is at high SNR and low MDG values. We also derived this conclusion previously in Section II-B. At low SNR and low MDG and at high SNR and high MDG the absolute determinant is small. Therefore, in these regions, measurements of SINR and σ_{mmse} with higher precision are required for proper SNR and σ_{mdg} estimation.

REFERENCES

- [1] R.-J. Essiambre and R. W. Tkach, "Capacity trends and limits of optical communication networks," *Proceedings of the IEEE*, vol. 100, no. 5, pp. 1035–1055, 2012.
- [2] T. Morioka, Y. Awaji, R. Ryf, P. Winzer, D. Richardson, and F. Poletti, "Enhancing optical communications with brand new fibers," *IEEE Communications Magazine*, vol. 50, no. 2, pp. s31–s42, 2012.
- [3] P. J. Winzer, "Optical networking beyond WDM," *IEEE Photonics Journal*, vol. 4, no. 2, pp. 647–651, 2012.
- [4] D. J. Richardson, J. M. Fini, and L. E. Nelson, "Space-division multiplexing in optical fibres," *Nature photonics*, vol. 7, no. 5, pp. 354–362, 2013.
- [5] K. Saitoh and S. Matsuo, "Multicore fiber technology," *Journal of lightwave technology*, vol. 34, no. 1, pp. 55–66, 2016.
- [6] J. M. Kahn and D. A. Miller, "Communications expands its space," *Nature photonics*, vol. 11, no. 1, pp. 5–8, 2017.
- [7] I. Cristiani, C. Lacava, G. Rademacher, B. J. Puttnam, R. S. Luis, C. Antonelli, A. Mecozzi, M. Shtaif, D. Cozzolino, D. Bacco *et al.*, "Roadmap on multimode photonics," *Journal of Optics*, vol. 24, no. 8, p. 083001, 2022.
- [8] P. J. Winzer, H. Chen, R. Ryf, K. Guan, and S. Randel, "Mode-dependent loss, gain, and noise in MIMO-SDM systems," in *2014 The European Conference on Optical Communication (ECOC)*. IEEE, 2014, pp. 1–3.
- [9] D. A. Mello, H. Srinivas, K. Choutagunta, and J. M. Kahn, "Impact of polarization-and mode-dependent gain on the capacity of ultra-long-haul systems," *Journal of Lightwave Technology*, vol. 38, no. 2, pp. 303–318, 2020.

- [10] M. Shtaif, C. Antonelli, A. Mecozzi, and X. Chen, "Challenges in estimating the information capacity of the fiber-optic channel," *Proceedings of the IEEE*, vol. 110, no. 11, pp. 1655–1678, 2022.
- [11] L. Zischler, R. S. Ospina, M. van den Hout, C. Okonkwo, and D. A. Mello, "Analytical model for the information rate of coupled SDM systems with MMSE equalizers," in *Optical Fiber Communication Conference*. Optica Publishing Group, 2025.
- [12] M. R. McKay, I. B. Collings, and A. M. Tulino, "Achievable sum rate of MIMO MMSE receivers: A general analytic framework," *IEEE Transactions on Information Theory*, vol. 56, no. 1, pp. 396–410, 2009.
- [13] K.-P. Ho and J. M. Kahn, "Mode-dependent loss and gain: statistics and effect on mode-division multiplexing," *Opt. Express*, vol. 19, no. 17, pp. 16 612–16 635, Aug 2011.
- [14] —, "Statistics of group delays in multimode fiber with strong mode coupling," *Journal of lightwave technology*, vol. 29, no. 21, pp. 3119–3128, 2011.
- [15] E. P. Wigner, "Characteristic vectors of bordered matrices with infinite dimensions," *Annals of Mathematics*, vol. 62, no. 3, pp. 548–564, 1955.
- [16] F. J. Dyson, "Statistical theory of the energy levels of complex systems," *Journal of Mathematical Physics*, vol. 3, no. 1, pp. 140–156, 1962.
- [17] M. L. Rosenzweig and R. H. MacArthur, "Graphical representation and stability conditions of predator-prey interactions," *The American Naturalist*, vol. 97, no. 895, pp. 209–223, 1963.
- [18] M. L. Mehta, *Random matrices*. Elsevier, 2004.
- [19] K.-P. Ho and J. M. Kahn, "Linear propagation effects in mode-division multiplexing systems," *Journal of lightwave technology*, vol. 32, no. 4, pp. 614–628, 2013.
- [20] P. J. Winzer and G. J. Foschini, "MIMO capacities and outage probabilities in spatially multiplexed optical transport systems," *Optics express*, vol. 19, no. 17, pp. 16 680–16 696, 2011.
- [21] C. Antonelli, A. Mecozzi, M. Shtaif, and P. J. Winzer, "Modeling and performance metrics of MIMO-SDM systems with different amplification schemes in the presence of mode-dependent loss," *Optics Express*, vol. 23, no. 3, pp. 2203–2219, 2015.
- [22] P. Serena, C. Lasagni, A. Bononi, C. Antonelli, and A. Mecozzi, "The ergodic GN model for space-division multiplexing with strong mode coupling," *Journal of Lightwave Technology*, vol. 40, no. 10, pp. 3263–3276, 2022.
- [23] C. Antonelli, M. Shtaif, and A. Mecozzi, "Modeling of nonlinear propagation in space-division multiplexed fiber-optic transmission," *Journal of Lightwave Technology*, vol. 34, no. 1, pp. 36–54, 2015.
- [24] M. Jankiraman, *Space-time codes and MIMO systems*. Artech House, 2004.
- [25] A. Efimov, "Spatial coherence at the output of multimode optical fibers," *Optics express*, vol. 22, no. 13, pp. 15 577–15 588, 2014.
- [26] C. Antonelli, A. Mecozzi, and M. Shtaif, "The delay spread in fibers for SDM transmission: dependence on fiber parameters and perturbations," *Optics express*, vol. 23, no. 3, pp. 2196–2202, 2015.
- [27] K. Shibahara, T. Mizuno, D. Lee, and Y. Miyamoto, "Advanced MIMO signal processing techniques enabling long-haul dense SDM transmissions," *Journal of Lightwave Technology*, vol. 36, no. 2, pp. 336–348, 2017.
- [28] L. Galdino, D. Semrau, D. Lavery, G. Saavedra, C. B. Czegledi, E. Agrell, R. I. Killey, and P. Bayvel, "On the limits of digital back-propagation in the presence of transceiver noise," *Optics Express*, vol. 25, no. 4, pp. 4564–4578, 2017.
- [29] A. Paulraj, R. Nabar, and D. Gore, *Introduction to space-time wireless communications*. Cambridge university press, 2003.
- [30] L. Zischler and D. A. Mello, "Analytic models for the capacity distribution in MDG-impaired optical SDM transmission," *Journal of Lightwave Technology*, 2025.
- [31] J. L. W. V. Jensen, "Sur les fonctions convexes et les inégalités entre les valeurs moyennes," *Acta mathematica*, vol. 30, no. 1, pp. 175–193, 1906.
- [32] G. Grimmett and D. Stirzaker, *Probability and random processes*. Oxford university press, 2020.
- [33] E. S. Chou and J. M. Kahn, "Successive interference cancellation on frequency-selective channels with mode-dependent gain," *Journal of Lightwave Technology*, vol. 40, no. 12, pp. 3729–3738, 2022.
- [34] S. Ö. Arık and J. M. Kahn, "Diversity-multiplexing tradeoff in mode-division multiplexing," *Optics Letters*, vol. 39, no. 11, pp. 3258–3261, 2014.
- [35] D. A. Mello, R. S. Ospina, H. Srinivas, K. Choutagunta, E. Chou, and J. M. Kahn, "Impact and mitigation of mode-dependent gain in ultra-long-haul SDM systems," in *Optical Fiber Communication Conference*. Optica Publishing Group, 2023, pp. M2B–6.
- [36] K.-P. Ho and J. M. Kahn, "Frequency diversity in mode-division multiplexing systems," *Journal of Lightwave Technology*, vol. 29, no. 24, pp. 3719–3726, 2011.
- [37] F. Bruyere and O. Audouin, "Penalties in long-haul optical amplifier systems due to polarization dependent loss and gain," *IEEE photonics technology letters*, vol. 6, no. 5, pp. 654–656, 1994.
- [38] A. N. Pilipetskii and E. A. Golovchenko, "Performance fluctuations in submarine WDM systems," *Journal of lightwave technology*, vol. 24, no. 11, pp. 4208–4214, 2006.
- [39] M. Shtaif and A. Mecozzi, "Polarization-dependent loss and its effect on the signal-to-noise ratio in fiber-optic systems," *IEEE Photonics Technology Letters*, vol. 16, no. 2, pp. 671–673, 2004.
- [40] A. Grami, *Introduction to digital communications*. Academic Press, 2015.
- [41] F. Buchali, F. Steiner, G. Böcherer, L. Schmalen, P. Schulte, and W. Idler, "Rate adaptation and reach increase by probabilistically shaped 64-QAM: An experimental demonstration," *Journal of lightwave technology*, vol. 34, no. 7, pp. 1599–1609, 2015.
- [42] T. Fehenberger, A. Alvarado, P. Bayvel, and N. Hanik, "On achievable rates for long-haul fiber-optic communications," *Optics Express*, vol. 23, no. 7, pp. 9183–9191, 2015.
- [43] A. Alvarado, T. Fehenberger, B. Chen, and F. M. Willems, "Achievable information rates for fiber optics: Applications and computations," *Journal of Lightwave Technology*, vol. 36, no. 2, pp. 424–439, 2018.
- [44] F. W. Olver, D. W. Lozier, R. F. Boisvert, and C. W. Clark, *NIST handbook of mathematical functions*. Cambridge university press, 2010.
- [45] R. S. Ospina, C. Okonkwo, and D. A. Mello, "DSP-based mode-dependent loss and gain estimation in coupled SDM transmission," in *Optical Fiber Communications Conference*. IEEE, 2020, pp. 1–3.
- [46] M. Van Den Hout, R. S. Ospina, S. van der Heide, J. C. Alvarado-Zacarias, J. E. Antonio-López, M. Bigot-Astruc, A. A. Correa, P. Sillard, R. Amezcua-Correa, D. A. Mello *et al.*, "Experimental validation of MDL emulation and estimation techniques for SDM transmission systems," in *2020 European Conference on Optical Communications (ECOC)*. IEEE, 2020, pp. 1–4.
- [47] R. S. Ospina, M. van den Hout, S. van der Heide, C. Okonkwo, and D. A. Mello, "Neural-network-based MDG and optical SNR estimation in SDM transmission," in *Optical Fiber Communication Conference*. Optica Publishing Group, 2021, pp. Th1A–20.
- [48] R. S. Ospina, M. Van den Hout, J. C. Alvarado-Zacarias, J. E. Antonio-López, M. Bigot-Astruc, A. A. Correa, P. Sillard, R. Amezcua-Correa, C. Okonkwo, and D. A. Mello, "Mode-dependent loss and gain estimation in SDM transmission based on MMSE equalizers," *Journal of Lightwave Technology*, vol. 39, no. 7, pp. 1968–1975, 2021.
- [49] R. S. Ospina, M. v. d. Hout, S. van der Heide, J. van Weerdenburg, R. Ryf, N. K. Fontaine, H. Chen, R. Amezcua-Correa, C. Okonkwo, and D. A. Mello, "MDG and SNR estimation in SDM transmission based on artificial neural networks," *Journal of Lightwave Technology*, vol. 40, no. 15, pp. 5021–5030, 2022.
- [50] R. S. Ospina, D. A. Mello, L. Zischler, R. S. Luís, B. J. Puttnam, H. Furukawa, M. van den Hout, S. van der Heide, C. Okonkwo, R. Ryf *et al.*, "Digital signal processing for MDG estimation in long-haul SDM transmission," *Journal of Lightwave Technology*, vol. 42, no. 3, pp. 1075–1084, 2023.
- [51] L. Zischler, R. S. Ospina, R. A. Colares, M. van den Hout, C. Okonkwo, R. B. Alencar, C. J. Bastos Filho, and D. A. Mello, "Estimating capacity and SNR loss induced by MDG using ANNs in optical SDM transmission," in *2024 SBFoton International Optics and Photonics Conference (SBFoton IOPC)*. IEEE, 2024, pp. 1–3.
- [52] S. O'Rourke, V. Vu, and K. Wang, "Eigenvectors of random matrices: a survey," *Journal of Combinatorial Theory, Series A*, vol. 144, pp. 361–442, 2016.
- [53] G. Livan, M. Novaes, and P. Vivo, "Introduction to random matrices theory and practice," *Monograph Award*, vol. 63, pp. 54–57, 2018.
- [54] F. J. Dyson, "The threefold way. Algebraic structure of symmetry groups and ensembles in quantum mechanics," *Journal of Mathematical Physics*, vol. 3, no. 6, pp. 1199–1215, 1962.
- [55] F. Clarke, "On the inverse function theorem," *Pacific Journal of Mathematics*, vol. 64, no. 1, pp. 97–102, 1976.